Reuleaux plasticity: improving Mohr-Coulomb and Drucker-Prager

W.M. Coombs[1] & R.S. Crouch

Durham University, School of Engineering and Computing Sciences,
South Road, Durham, DH1 3LE, United Kingdom.

ABSTRACT

The yielding of soil exhibits both a Lode angle dependency and a dependency on the intermediate principal stress. Ignoring these leads to a loss of realism in geotechnical analysis, yet neither of the widely used Mohr-Coulomb (M-C) or Drucker-Prager (D-P) models include both. This paper presents a simple pressure-dependent plasticity model based on a modified Reuleaux (mR) triangle which overcomes these limitations and yet (like the M-C and D-P formulations) allows for an analytical backward-Euler stress integration solution scheme. This latter feature is not found in more sophisticated (and computationally expensive) models. The mR deviatoric function is shown to provide a significantly improved fit to experimental data when compared with the M-C and D-P functions. Finite deformation finite-element analysis of the expansion of a cylindrical cavity is presented, verifying the use of the mR constitutive model for practical analyses.

Keywords: geomaterials, computational plasticity, analytical stress return, Mohr-Coulomb, Drucker-Prager

1 INTRODUCTION

Accurate and fast numerical analysis methods, using tools such as finite-elements, are now widely and successfully used when tackling complex geomechanical problems. The appropriate choice of constitutive model is essential for such analyses [14].

The non-associated perfect plasticity model presented here overcomes the limitations of the Drucker-Prager (D-P) and Mohr-Coulomb (M-C) models, yet requires no additional material constants. The D-P yield surface exhibits no Lode angle dependency, θ. The M-C surface has no sensitivity to the intermediate principal stress, σ_2. Yet multiaxial experiments show that both factors influence yielding and peak stresses. Inclusion of these dependencies in constitutive models is necessary in order to capture properly the deformation of geotechnical structures [2]. The attraction of the proposed model is the improved fit to deviatoric yielding (the formulation has a sensitivity to both θ and σ_2) and a fast, one-step, implicit stress integration scheme.

This paper uses a tension positive convention with the following ordering of the principal stresses $\sigma_1 \leq \sigma_2 \leq \sigma_3$.

2 SOIL DEVIATORIC YIELDING

Particulate materials, such as soils, fractured rocks, grains and powders, experience permanent deformations which are dependent on the imposed hydrostatic pressure. M-C and D-P [8] are two of the most widely used pressure-sensitive constitutive models in the literature which can capture this behaviour in an idealised way. The M-C criterion assumes that plastic frictional sliding will occur once the minor principal stress falls below some proportion of the major principal stress. This can be defined using the following yield function

$$f = k\sigma_3 - \sigma_1 - \sigma_c = 0, \qquad \text{where} \qquad (1)$$
$$k = \frac{1+\sin(\phi)}{1-\sin(\phi)} \quad \text{and} \quad \sigma_c = 2c\sqrt{k}.$$

ϕ is the internal friction angle, c the cohesion and σ_c defines the uniaxial compressive yield strength[2]. The constitutive models examined in this paper may also be defined using Haigh-Westergaard cylindrical coordinates

$$\xi = \text{tr}[\sigma]/\sqrt{3}, \qquad \rho = \sqrt{2J_2} \qquad \text{and} \qquad (2)$$
$$\theta = \frac{1}{3}\arcsin\left(\frac{-3\sqrt{3}}{2}\frac{J_3}{J_2^{3/2}}\right) \quad \in \left[-\pi/6, \pi/6\right].$$

Here $J_2 = (\text{tr}[s]^2)/2$, $J_3 = (\text{tr}[s]^3)/3$, $[s] = [\sigma] - \xi[I]/\sqrt{3}$ and $[I]$ denotes the 3 by 3 identity matrix.

The M-C normalised deviatoric radius, $\overline{\rho}$, (the ratio of the yield radius to that at the compression meridian $\overline{\rho} = \rho/\rho_c$) or Lode angle dependency (LAD), as shown in Figure 1, can be expressed as

$$\overline{\rho}(\theta) = \frac{\sqrt{3}\overline{\rho}_e}{2a_1\sin(5\pi/6 - a_2 - \theta)} \qquad (3)$$

[1]corresponding author: William Coombs, Durham University, School of Engineering and Computing Sciences, South Road, Durham, DH1 3LE, United Kingdom. w.m.coombs@durham.ac.uk

[2]Note, that setting a non-zero cohesion is equivalent to assuming some initial hydrostatic stress in the material, given by $p = c\cot(\phi)$.

where $a_2 = \arcsin\left(\sqrt{3}\overline{\rho}_e/2a_1\right)$, $a_1 = \sqrt{1+(\overline{\rho}_e)^2-\overline{\rho}_e}$ and $\overline{\rho}_e$ is the normalised deviatoric radius on the extension meridian to that on the compression meridian. This allows the M-C yield function (1) to be written as

$$f = \rho - \alpha\overline{\rho}(\theta)\left(\xi - \xi_c\right) = 0, \tag{4}$$

where $\xi_c = c\sqrt{3}\cot(\phi)$ is the hydrostatic tensile yield strength (the intersection of the yield surface with the hydrostatic axis) and $\alpha = -\tan(\phi)$ defines the opening angle of the yield surface on the compression meridians.

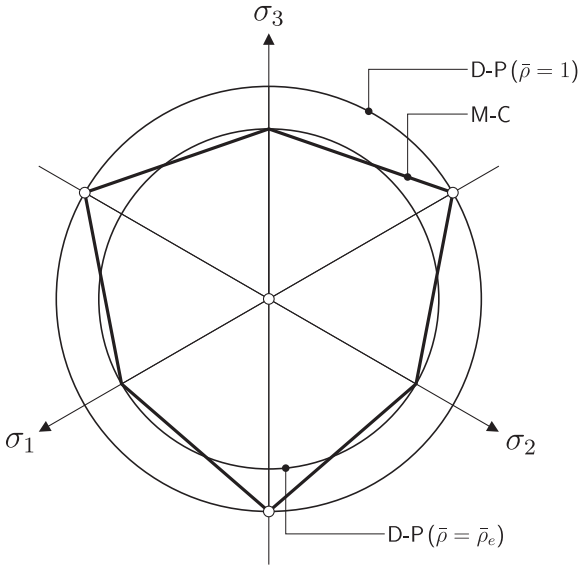

Figure 1. M-C and D-P deviatoric sections.

The D-P [8] criterion provides a smooth approximation to the six-faceted M-C yield function. It is defined such that plastic yielding will occur once ρ reaches some ratio of the hydrostatic stress (independent of θ)

$$f = \rho - \alpha\overline{\rho}(\xi - \xi_c) = 0. \tag{5}$$

Here $\overline{\rho}$ is a constant, as shown in Figure 1, defining a circular cone with its axis centered on the hydrostatic axis. Setting $\overline{\rho} = 1$ or $\overline{\rho} = \overline{\rho}_e$ allows (5) to coincide with the M-C criterion at the extension or compression meridians. When intersecting at the extension meridians, $\overline{\rho}_e$ is obtained from ϕ as

$$\overline{\rho}_e = (2+k)/(2k+1). \tag{6}$$

2.1 Modified Reuleaux

The Reuleaux triangle can trace its origins back to the 1830s where the shape was used in cam-actuated steam engine regulators. It was not until 1876 that the first written discussion of the geometry appears to have been provided by Franz Reuleaux [15]. The Reuleaux triangle belongs to a family of curved shapes of constant breadth (that is, rolling polygons which maintain a constant height)[3]. The six-fold symmetric shape is formed through three equal circular arcs projected from the triangle's corners.

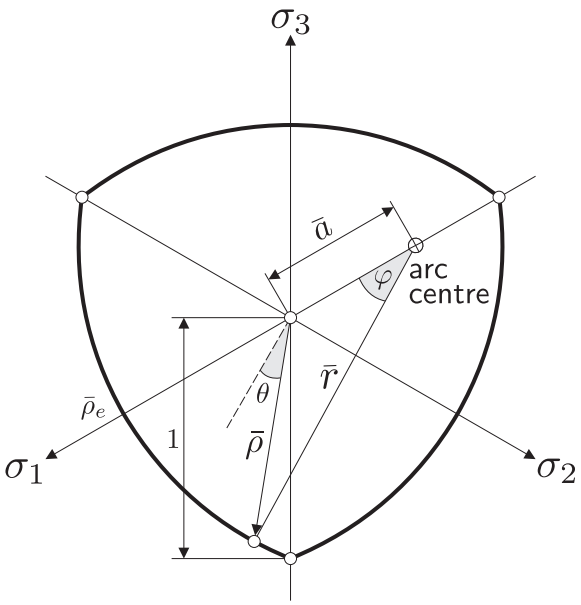

Figure 2. Modified Reuleaux triangle ($\overline{\rho}_e = 0.8$).

Coombs *et al.* [5] extended the Reuleaux triangle such that the arc centres are allowed to translate along the extension meridians. This modified Reuleaux (mR) triangle is shown in Figure 2. From this figure, we find that the mR Lode angle dependency is

$$\overline{\rho}(\theta) = \sqrt{\overline{a}^2 + \overline{r}^2 - 2\overline{a}\,\overline{r}\cos(\varphi)}, \quad \text{where}$$

$$\overline{r} = \frac{\overline{\rho}_e^2 - \overline{\rho}_e + 1}{2\overline{\rho}_e - 1}, \qquad \text{and} \qquad \overline{a} = \overline{r} - \overline{\rho}_e. \tag{7}$$

The arc angle, φ, is defined as

$$\varphi = \frac{\pi}{6} + \theta - \arcsin\left(\frac{\overline{a}\sin(5\pi/6-\theta)}{\overline{r}}\right). \tag{8}$$

Although the mR criterion allows control of $\overline{\rho}_e$ independent of ϕ, in the absence of multiaxial data, $\overline{\rho}_e \in [0.5, 1]$ can be defined using (6) such that the mR triangle coincides with M-C at the extension meridians.

[3] Other examples of these polygons that roll with a constant height are the sterling twenty and fifty pence coins.

The mR cone is formed by combining (4) and (7), yielding a frictional cone with linear meridians and a mR deviatoric section, as shown in Figure 3. It is widely accepted that associated frictional plasticity models overestimate the dilation seen in particulate media. To overcome this shortfall, Coombs and Crouch [4] introduced a non-associated plastic flow (NAF) rule with the angle of plastic dilation less than ϕ. Combining this with a linear hyperelastic relationship gives rise to the NAF mR constitutive model.

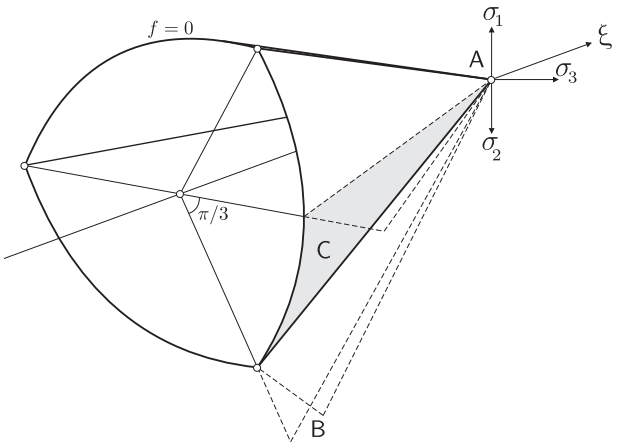

Figure 3. Modified Reuleaux yield surface.

Coombs *et al.* [5] and Coombs and Crouch [4] made use of an implicit backward Euler (BE) stress return scheme (see Simo and Hughes [17]) for the case of associated and NAF, respectively. These previous papers used the concept of energy mapped stress space, originally formulated by Crouch *et al.* [7]. This space allows the implicit stress return to be constructed using purely Euclidean geometric methods. That is, the closest point (lying on the mR surface) to a point outside the surface, may be found analytically by determining the appropriate root of a quartic equation. Figure 3 identifies the model's three return regions: A apex, B corner and C non-planar surface return. All regions allow for a fast, fully robust, analytical stress return, eliminating the stability problems which are often seen in iterative solution schemes..

3 MODEL COMPARISONS

3.1 Experimental observations: θ and σ_2

The M-C, D-P and mR deviatoric functions are compared with experimental data from (i) Monterey sand (MS) [12] and (ii) Kaolin (K) [1] in Figure 4. There is evidence elsewhere that many materials exhibit dependencies on both θ and σ_2 [3,9,11,13,16]. The left of Figure 4 compares experimental data in terms of θ-$\overline{\rho}(\theta)$. D-P has no dependence on θ, and therefore provides a poor fit to the experimental data.

Table 1 provides a quantitative measure of the error between $\overline{\rho}$ and the experimental data for the four models. The error is calculated as

$$\text{error} = \frac{1}{n}\sum_{i=1}^{n} |\rho_i - \overline{\rho}(\theta_i)|, \tag{9}$$

where i denotes the experimental data point (out of a total of n) with ρ_i and θ_i being the experimental normalised deviatoric radius and Lode angle, respectively. mR provides an improved fit over M-C and D-P for all of the materials. Note that, in Figure 4 (ii) $\overline{\rho}_e$ for the mR was not set equal to $\overline{\rho}_e$ for M-C.

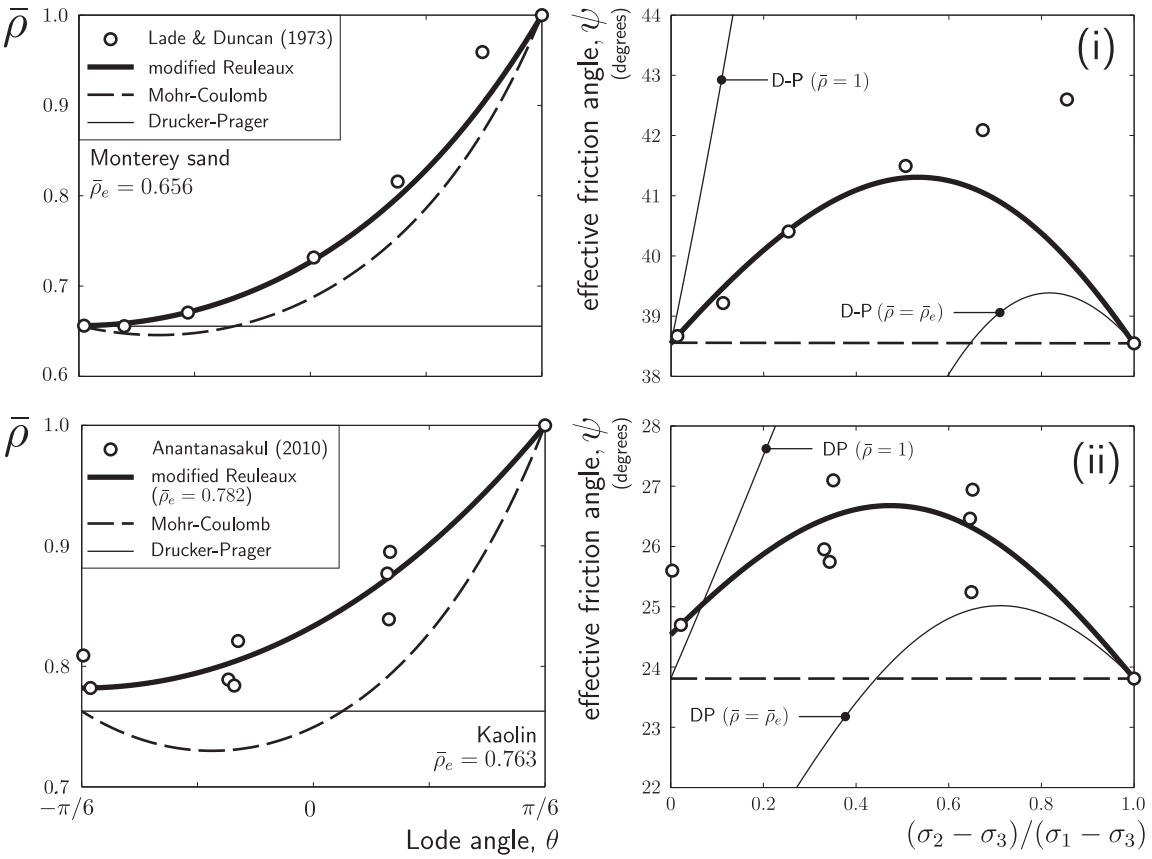

Figure 4. Comparison of M-C, D-P and mR with experimental data on (i) Monterey sand [12] and (ii) Kaolin [1].

The right of Figure 4 compares experimental data in terms of ratio of the intermediate principal stress $b = (\sigma_2 - \sigma_3)/(\sigma_1 - \sigma_3)$ versus the effective friction angle ψ, where the latter is calculated from the expression given by Griffiths [10]

$$\psi = \arcsin\left(\frac{\sqrt{3}\eta\cos(\theta)}{\sqrt{2} + \eta\sin(\theta)}\right), \qquad (10)$$

with $\eta = (\rho/\xi)^4$. The experimental data show a dependence on the intermediate principal stress σ_2. The D-P model can only coincide with M-C at a single b. If this occurs at $b = 0$ then the deviatoric radius significantly over-estimates the effective friction angle, whereas if this occurs at $b = 1$, then it under estimates ψ. Of the three formulations considered here, only the mR model, having a dependency on both θ and σ_2, is able to qualitatively reproduce the experimentally observed material behaviour.

model		M-C	D-P ($\bar{\rho} = 1$)	D-P ($\bar{\rho} = \bar{\rho}_e$)	mR
material	MS	0.0562	0.2060	0.1380	0.0342
	K	0.0422	0.1170	0.0807	0.0113

Table 1. Lode angle dependency errors.

3.2 Numerical analysis

This section presents results from simulating the internal expansion of a cylindrical cavity using a two-dimensional plane strain finite deformation finite-element analysis. The cavity has an internal radius of $a_0 = 0.042$m and is modelled using a 3° slice with a fixed outer radius at $b_0 = 80$m.

The three constitutive models, in addition to a NAF frictional cone based on a Willam-Warnke (W-W) deviatoric section[5] [18], were implemented within an updated Lagrangian logarithmic strain-Kirchhoff stress finite deformation framework, see Coombs *et al.* [4,6] for more details.

[4]Note, on the compression meridian ϕ and ψ are equivalent and equal.

[5]Note it is not possible to form an analytical stress return for the W-W model, the implicit backward Euler stress return can require multiple iterations to find convergence.

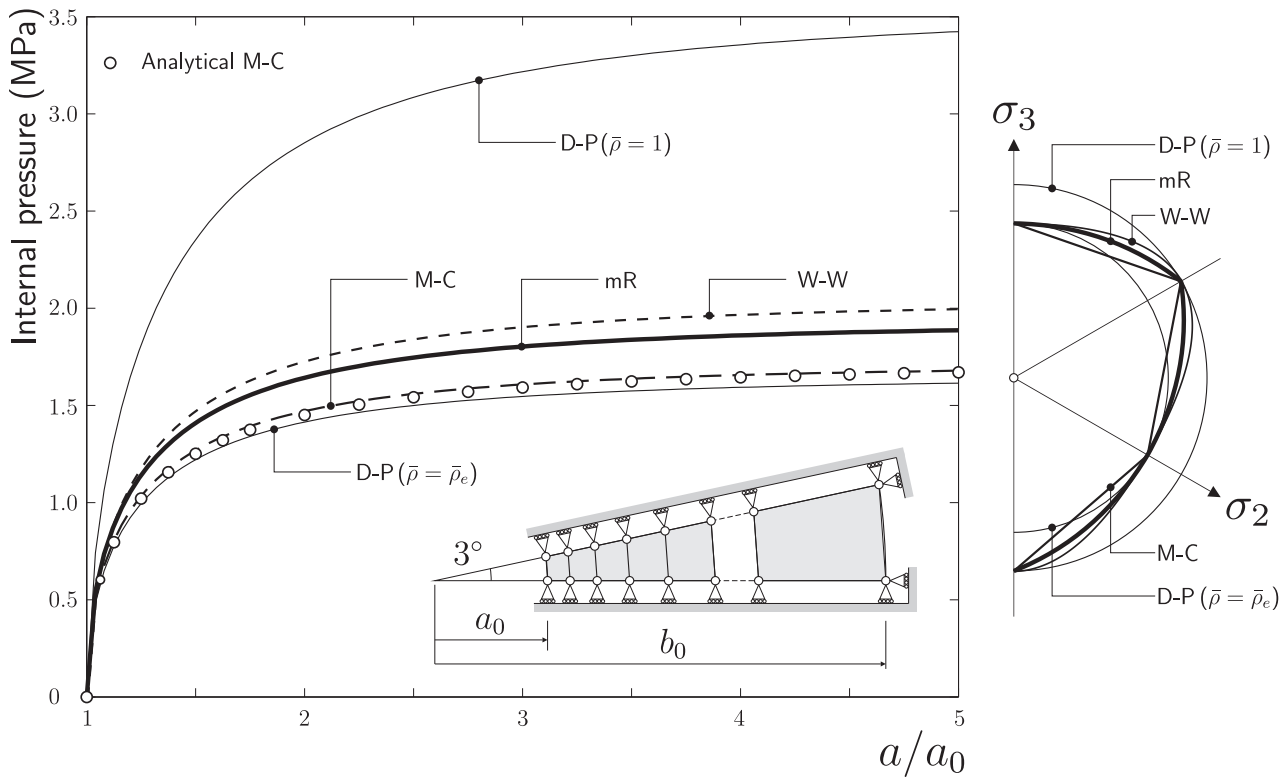

Figure 5. Plane strain cavity expansion internal pressure-expansion response.

All models used a Young's modulus of 100MPa and a Poisson's ratio of 0.2 for the model's elastic parameters. The friction and dilation angles were set to $\pi/6$ and $\pi/12$, respectively, with the normalised deviatoric radius under triaxial extension for mR coinciding with that of M-C ($\overline{\rho}_e = 0.7143$) and a cohesion of 50kPa. Two forms of D-P were modeled, such that they coincided with M-C at the compression ($\overline{\rho} = 1$) and extension ($\overline{\rho} = \overline{\rho}_e$) meridians, as shown on the right of Figure 5.

model	$\sum$(NRit)	max(NRit)	n_{pgp}	t/t_{MC}	P_{max}
					(kPa)
M-C	488	5	146	1	1678.5
D-P($\bar{\rho} = 1$)	499	5	142	1.004	3423.2
D-P($\bar{\rho} = \bar{\rho}_e$)	497	5	142	0.999	1614.4
mR	486	5	144	1.053	1886.6
W-W	479	5	144	1.419	2046.7

Table 2. Plane strain cavity expansion results.

50 four-noded plane strain quadrilateral elements with four point Gaussian quadrature model the problem. The length of the elements was progressively increased by a factor 1.16 from the inner to the outer surface. During the analysis the internal radius was expanded to 0.21m (that is, 5× its original radius) via 100 equal displacement-controlled increments. Figure 5 presents the internal pressure-displacement response, where a/a_0 is the ratio of the current to the original internal radius. The numerical solution for M-C shows excellent agreement with the analytical solution provided by Yu & Houlsby [19].

Table 2 gives the total and maximum (for any load-step) number of Newton-Raphson iterations (NRit), the number of plastic material points at the end of the analysis (n_{pgp}), the ratio of the analysis time to that of M-C (t/t_{MC}) and the maximum internal pressure (P_{max}). The total number of iterations differs only slightly between the four models, and the maximum is the same for the models. Although the mR model provides significantly increased realism over the M-C and D-P models, the analysis time is only increased by 5.3%. The W-W model provides a similar level of realism to that of mR but the analysis time increases by 41.9% due to the multiple iterations required for each material point stress return. The mR model has a higher maximum pressure than M-C, as the deviatoric section encloses the M-C (coinciding only at $\theta = \pm\pi/6$). Changing the radius of the D-P model from $\overline{\rho}_e$ to 1 increases the maximum pressure by 212%, demonstrating the consequence of selecting an inappropriate normalised deviatoric radius[6] (or friction angle).

[6]This point was highlighted by Potts and Zdravkovic [14] for the analysis of a rigid footing with the modified Cam Clay constitutive model.

4 OBSERVATIONS

The simple mR model has been shown to provide improved realism (having a dependence on both θ and σ_2) over the M-C and D-P functions when compared with multi-axial experimental data. This is achieved without the computational overhead associated with more sophisticated models (such as the W-W formulation) by allowing for an analytical backward Euler stress return. Thus the mR constitutive model overcomes the inadequacies inherent in, and provides a suitable replacement for, both M-C and D-P in practical geotechnical numerical analyses. For example, it allows engineers to undertake more detailed 3D analyses where more sophisticated models still demand unacceptably long runtimes. The formulation is simple enough to code; it can be easily incorporated in commercial finite-element programs.

REFERENCES

[1] P Anantanasakul, *Three-dimensional experiments and modelling of anisotropic clay*, PhD. Thesis, Oregon State University (2010).

[2] T Benz, M Wehnert, and PA Vermeer, *A Lode angle dependent formulation of the Hardening Soil model*, 12th IACMAG, 2008, pp. 653–660.

[3] M Cai, *Influence of intermediate principal stress on rock fracturing and strength near excavation boundaries-Insight from numerical modeling*, Int. J. of Rock Mechanics and Mining Sciences 45 (2008), 763–772.

[4] WM Coombs and RS Crouch, *Non-associated Reuleaux plasticity: Analytical stress integration and consistent tangent for finite deformation mechanics*, Comput. Meth. Appl. Mech. Engrg. 200 (2011), 1021–1037.

[5] WM Coombs, RS Crouch and CE Augarde, *Reuleaux plasticity: Analytical backward Euler stress integration and consistent tangent*, Comput. Meth. Appl. Mech. Engrg. 199 (2010), 1733–1743.

[6] WM Coombs, RS Crouch and CE Augarde, *70-line 3D finite deformation elastoplastic finite-element code*. In: T Benz and S Nordal (eds.), 7th European Conference on Numerical Methods in Geoetchnical Engineering (2010), 151–156.

[7] RS Crouch, H Askes, and T Li, *Analytical CPP in energy-mapped stress space: application to a modified Drucker-Prager yield surface*, Comput. Meth. Appl. Mech. Engrg. 198 (5–8) (2009), 853–859.

[8] DC Drucker and W Prager, *Soil mechanics and plastic analysis or limit design*, Quart. Appl. Math. 10 (1952), 157–164.

[9] E Fjær and H Ruistuen, *Impact of the intermediate principal stress on the strength of heterogeneous rock*, Journal of Geophysical Research 107 (2002).

[10] DV Griffiths, *Failure criteria interpretation based on Mohr-Coulomb friction*, ASCE J. Geotech. Eng. 116 (6) (1990), 986–999.

[11] K Issen and V Challa, *Influence of the Intermediate Principal Stress on Compaction Localization Conditions*, The 41st U.S. Symposium on Rock Mechanics (USRMS), June 17–21, 2006.

[12] PV Lade and JM Duncan, *Cubical triaxial tests on conhesionless soil*, J. Soil Mech. Found. Div. ASCE 99 (1973), 193–812.

[13] AP Morris and DA Ferrill, *The importance of the effective intermediate principal stress (σ_2') to fault slip patterns*, Journal of Structural Geology 31 (2009), 950–959.

[14] DM Potts and L Zdravković, *Finite element analysis in geotechnical engineering: application*, Thomas Telford Publishing, London, 2001.

[15] F Reuleaux, *The kinematics of machinery: Outlines of a theory of machines*, Macmillan and Co., London, 1876.

[16] A Säyao and YP Vaid, *Effect of intermediate principal stress on the deformation response of sand*, Can. Geotech. J. 33 (1996), 822–828.

[17] JC Simo and TJR Hughes, *Computational inelasticity*, Springer, New York, 1998.

[18] KJ Willam and EP Warnke, *Constitutive model for the triaxial behaviour of concrete*, Proceedings of the May 17-19 1974, International Association of Bridge and Structural Engineers Seminar on Concrete Structures Subjected to Triaxial Stresses, held at Bergamo Italy, 1974.

[19] HS Yu and GT Houlsby. *Finite cavity expansion in dilatant soils: Loading analysis*, Géotechnique 41, (1991), 173–183.